Available online at www.sciencedirect.com
SCIENCE DIRECT
Journal of Power Sources 155 (2006) 253–263
JOURNAL OF POWER SOURCES
www.elsevier.com/locate/jpowsour

Stability of platinum based alloy cathode catalysts in PEM fuel cells

Héctor R. Colón-Mercado, Branko N. Popov *

Center for Electrochemical Engineering, Department of Chemical Engineering, University of South Carolina, Columbia, SC 29208, USA

Received 15 March 2005; received in revised form 6 May 2005; accepted 9 May 2005
Available online 20 June 2005

Abstract

Corrosion and surface area changes of platinum (Pt) based catalysts supported on carbon were evaluated using an accelerated durability test (ADT). The results obtained using the ADT were correlated to the performance of the Pt based catalysts in the fuel cell. The catalytic activity and dissolution rate of the alloying metal from the Pt-alloy catalysts were estimated in the same time domain. A strong correlation was observed between the amount of the alloying metal dissolved and the oxygen reduction reaction (ORR) activity of the Pt-alloy catalysts. The Pt catalyst exhibited loss of active surface area, and a resulting decrease in the ORR activity was observed. The Pt/C and Pt–Co/C catalysts showed similar behavior in both ADT and in the fuel cell testing. Cross-sectional studies by electron microprobe analysis of the membrane electrode assembly after fuel cell testing revealed cobalt dissolution followed by diffusion into the membrane.

Keywords: PEM fuel cell; Oxygen reduction; Platinum alloy; Dissolution; Cathode stability; Activity

1. Introduction

Highly dispersed platinum crystallites on a conductive support that has a high surface area, such as carbon black, is used as electrocatalyst for hydrogen oxidation and oxygen reduction reactions [1,2]. The use of highly dispersed crystallites on high surface area carbon particles increases both the active surface area and the electrocatalytic activity of the catalyst. The overpotential of the anode when operated on neat hydrogen is on the order of tens of microvolts. However, at the cathode, the overpotential caused by slower kinetics is in excess of 300 mV from the thermodynamic potential for oxygen reduction reactions (ORR), even when pure Pt is used [1]. The search for more active and less expensive ORR catalysts with better stability than Pt based catalysts has led to the development of binary and ternary Pt-alloys [3–5].

Studies of ORR on Pt-alloys supported on carbon black for phosphoric acid fuel cells (PAFC) and polymer electrolyte fuel cells (PEFC) have indicated the enhancement in activity as a result of the shortening of the distance to the nearest neighbor by alloying [3–5]. Other properties intrinsic to Pt-alloys have been attributed to the increase in activity. This includes the exposure of a more active vicinal plane (1 0 0) on dispersed platinum particles. The exposure of the more active plane is believed to take place during the heat treatments used to induce alloy formation in the particles [6]. Mukerjee et al. [7] and Toda et al. [8] explains the enhancement on the basis of the augmentation of Pt d-vacancy and the effect of higher affinity for the oxygenated species on the catalyst.

The loss of activity in PAFC during testing has been explained by the loss of active surface area due in part to particle agglomeration [9–13] and the leaching of the alloying metal into the electrolyte [14–16]. The acid environment in the PEMFC is different from that of PAFCs because the anions of the perfluorinated sulfonic acid polymer are only weakly adsorbed to the Pt surface. In addition, the operating temperature of the PEMFC is more than half that of the PAFC. As a result, a better stability is expected for the catalysts in the PEMFC. Wilson et al. studied the particle growth for Pt catalyst after testing the catalyst in a fuel cell for 4000 h of continuous operation. Wilson et al. found that approximately 60% of the active surface area was lost [17]. Other studies in wet cells have shown that after the catalysts have been

* Corresponding author. Tel.: +1 803 777 7314; fax: +1 803 777 8265.
E-mail address: popov@engr.sc.edu (B.N. Popov).

0378-7753/$ – see front matter © 2005 Elsevier B.V. All rights reserved.
doi:10.1016/j.jpowsour.2005.05.011

briefly immersed in an acid electrolyte, a skin consisting of a monolayer of pure Pt forms on the surface of the Pt-alloys [8,18,19]. These results indicate the dissolution of the metal from the cathode catalyst during the cell operation. In our previous work [20] we developed an accelerated durability test (ADT), which was used to identify the reasons for the decrease in performance of Pt and Pt-alloy catalysts.

The objective of this work was to study the different commercially available platinum bimetallic catalysts by using the ADT, and then to correlate the results to the actual behavior of the Pt based catalysts in the fuel cell.

2. Experimental

2.1. Electrochemical measurement of the activity for the ORR

A glassy carbon rotating disk electrode (GCRDE) was used for the determination of the active surface area and evaluation of the catalyst's electrocatalytic activity. The experiments were performed in 0.3 M H_2SO_4 solution at room temperature, where a saturated calomel electrode (SCE) was used as the reference electrode. The catalyst ink was prepared by ultrasonically blending the catalyst (2.8 mg) with 1 mL of distilled water for 5 min in a Branson Ultrasonic Cleaner. The ink (10 μL) was then placed on the glassy carbon surface of the RDE. After drying, a catalyst loading of ∼28 μg was achieved on the GCRDE. A volume of 5 μL of a mixture of Nafion solution (5 wt.% from Aldrich) and isopropyl alcohol (1:20) was applied on the dry catalyst to ensure better adhesion of the catalyst on the glassy carbon surface. The experiments were performed using a three-neck round bottom flask containing 0.3 M H_2SO_4 solution. Initially, in order to clean the surface of the catalyst, the system was purged with N_2 and cycled between 1.24 and −0.03 V versus normalized hydrogen electrode (NHE) at a scan rate of 50 mV s^{-1}. Next, the electrode was polarized by using a 5 mV s^{-1} scan rate in order to evaluate the electrochemically active surface area.

Hydrodynamic voltammograms (at rotation rates varied from 300 to 3000 rpm in 0.3 M H_2SO_4 solution saturated with O_2) for ORR were recorded between 1.04 and 0.24 V versus NHE at a scan rate of 5 mV s^{-1}. The Koutecky–Levich equation [21] is used to calculate the kinetic currents

$$\frac{1}{i} = \frac{1}{i_k} + \frac{1}{i_l} + \frac{1}{i_f} = \frac{1}{nFkC_0} + \frac{1}{0.62nFAD_O^{2/3}\omega^{1/2}\nu^{-1/6}C_0} + \frac{L}{nFc_fD_f} \quad (1)$$

where 'C_0' is the bulk concentration, 'ν' the kinematic viscosity, 'ω' the rotation rate in radians per second, 'D_O' the diffusion of O_2 in the bulk, 'A' the surface area, 'n' the number of electrons exchanged in the electrochemical reaction, 'F' the Faraday's constant, 'L' the film thickness, 'c_f' the reactant concentration in the Nafion film and 'D_f' is the diffusion constant in the Nafion film. Since the film thickness was reduced to the extent that the Nafion film diffusion limited current density, 'i_f' becomes significantly larger than the kinetically limited current density 'i_k' and diffusion limited current density, 'i_l', the influence of 'i_f' on the measured current in our experiments was negligible. By plotting i^{-1} versus $\omega^{-1/2}$ and extending the regression line, the y-intercept or the inverse of the kinetic current can be calculated.

Table 1
Commercially available platinum based catalysts considered in this study

Catalyst	Metal	Atomic ratio (Pt:M)
20Pt/C	Pt	–
$20Pt_1Ni_1$/C	Pt:Ni	1:1
$20Pt_3Ni_1$/C	Pt:Ni	3:1
$20Pt_1Co_1$/C	Pt:Co	1:1
$20Pt_3Co_1$/C	Pt:Co	3:1
$20Pt_1Fe_1$/C	Pt:Fe	1:1
$20Pt_1V_1$/C	Pt:V	1:1

Metal loading is 20 wt.% on Vulcan XC-72.

2.2. Electrode preparation

The commercial catalysts Pt_xM_1 supported on Vulcan XC-72 (20 wt.% metal loading) were purchased from E-TEK (see Table 1). The electrodes were prepared by ultrasonically blending 0.2 g of carbon catalyst, 0.706 g of Nafion solution (5 wt.% from Aldrich) and 4 mL of isopropyl alcohol for 1 h. The catalyst solution was sprayed on the surface of a single-sided uncatalyzed gas diffusion layer (GDL) by using a Paasche air brush. The GDL was obtained from ETEK. The area of the electrode was fixed at 10 cm^2. After the catalyst was sprayed, the electrode was dried at 80 °C for 30 min. The process was repeated until a total metal loading of 0.4 mg cm^{-2} was achieved.

2.3. Accelerated durability test

The ADT cell consists of a three-electrode system, which includes a reference electrode, a platinum mesh counter electrode and a catalyst-coated GDL as a working electrode. To avoid any chloride contamination, Hg/Hg_2SO_4 electrode was used as a reference electrode. The ADT experiments were carried out by immersing the electrodes in 200 mL of 0.3 M H_2SO_4 solution, which mimics the environment of the electrode–membrane interface of the cathode side. The difference between the actual fuel cell test using a membrane electrode assembly (MEA) and ADT is that in the case of MEA only the catalyst, which is in contact with the membrane is active. Also, the proton electromigration and diffusion (the proton mobility) is limited due to the presence of a solid polymer electrolyte interfacing the cathode and the anode. In the case of ADT, the entire active surface of the catalyst is exposed and high proton mobility in the liquid results in more severe catalyst corrosion than that observed in the MEA. Under these conditions, the deterioration of the catalysts is accelerated. A fixed potential of 0.9 and 0.8 V versus NHE

was applied to the working electrode (the catalyst-coated GDL) and the responding current was recorded by using an Arbin instrument (Model No. BT-2043).

During the ADT, approximately 3 mL of the test solution (0.3 M H_2SO_4) was taken out periodically and analyzed using atomic absorption spectroscopy (AAS, Perkin-Elmer 3300). Using this procedure, it was possible to estimate the dissolution rate of the non-noble metal catalyst in the solution as a function of time and applied potential. The experiment was terminated after approximately 480 h, which is the point where the ORR current reaches steady state.

Also, an EG&G PAR model 273 potentiostat was used to record cyclic voltammograms (CV) on an identical cathode electrode. A similar three-electrode system as that described above was used for the study. In order to avoid interference of the ORR, the CVs were recorded in 0.3 M H_2SO_4 solution purged with nitrogen. The CVs were recorded as a function of time at the scan rate of 5 mV s^{-1} in a potential window of 1.24 to −0.03 V versus NHE for the duration of 1100 cycles.

2.4. Fuel cell testing

The actual performance of the catalysts was studied in a fuel cell. For these experiments, the most promising platinum alloy (20 wt.% Pt_3Co on Vulcan XC-72) catalyst was selected and compared with the pure platinum catalyst (19.6 wt.% Pt on Vulcan XC-72). The cathode catalyst ink was prepared by ultrasonically blending a mixture of 0.2 g of catalyst, 1.33 g of Nafion solution and 4 mL of isopropyl alcohol in a Branson Ultrasonic cleaner for 1 h. The catalyst solution was then sprayed onto the surface of a single-sided uncatalyzed gas diffusion layer obtained from E-TEK. After the catalyst was sprayed, the electrode was dried at 80 °C for 30 min. The process was repeated until a total metal loading of 0.4 mg cm^{-2} was achieved. After loading the catalyst, a thin layer of Nafion (0.4 mg cm^{-2}) was applied on the surface of the electrode to improve the catalyst membrane adhesion. The anode electrode used was a commercial E-TEK electrode (30 wt.% Pt) with a loading of 0.5 mg cm^{-2} of Pt on the GDL. As in the case of the cathode electrode, a layer of Nafion was applied on the surface of the anode. MEAs with an area of 10 cm^2 were fabricated by hot pressing the cathode and anode electrodes to a pre-conditioned membrane (Nafion 112 form Alfa Aesar) at 140 °C at 533.8 kPa for 3 min.

The performance of the MEAs was studied as a function of time at atmospheric pressure and at an operating temperature of 75 °C. Pure oxygen gas humidified at 75 °C and pure hydrogen gas humidified at 77 °C were passed to the cathode and the anode compartment, respectively. The cells were run at a constant load of 1 A cm^{-2}, where the CVs were performed periodically in order to estimate the change of the electroactive surface area as a function of time.

2.5. Physical characterization

Transmission electron microscopy (TEM, Hitachi H-8000) was used to determine the change in particle size of catalyst before and after the test. Backscattering scanning electron microscope (BSEM) and electron microprobe analysis (EMPA, EMPA Cameca SX50) were used to determine the distribution of the elements across the MEA before and after test. X-ray diffraction analysis (XRD, Rigaku 405S5 with Cu Kα as the ration source) was carried out on the samples to examine the change of the structure of the catalyst after the ADT test.

3. Results and discussion

3.1. Electrochemical measurement on the activity for the ORR

Fig. 1 shows a typical CV obtained for 20% Pt/C compared to the CVs obtained for 20% Pt_3Co/C and 20% PtCo/C alloys. The two peaks observed correspond to the oxidation–reduction of Pt and desorption–adsorption of hydrogen on the Pt surface.

In the case of Pt-alloys, a potential shift of approximately 80 mV occurs at 0.7 V versus NHE where the onset of oxide formation is observed. The observed positive shift indicates the creation of a weakly adsorbed oxide layer on the Pt surface, which is easier to reduce, and. increases the ORR activity of the Pt-alloys as discussed by Paulus et al. [23]. The hydrogen adsorption–desorption potential in the region between 0.05 and 0.25 V versus NHE is similar for both Pt and Pt-alloys. However, a reduction in the hydrogen underpotential deposition (H_{UPD}) area is observed in the case of Pt-alloys. This reduction can be attributed to the increase in particle size. Pt-alloys with 75 at.% Pt (i.e., 20Pt_3Co/C) show a similar strong and weak H_{UPD} peak, while Pt-alloys

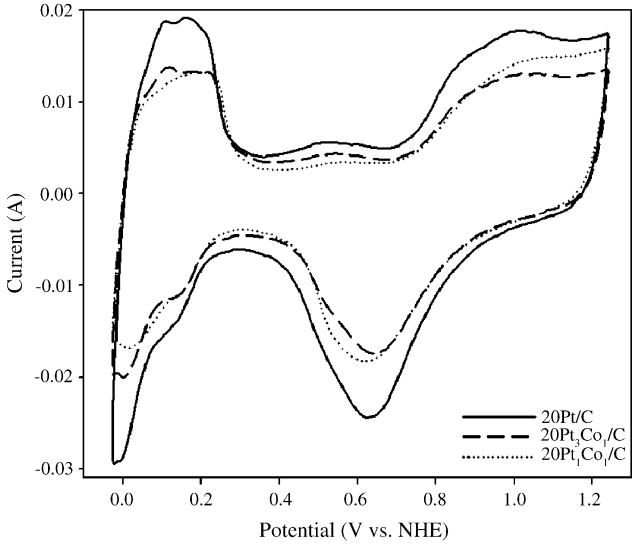

Fig. 1. Voltammograms for Pt and Pt-alloys in 0.3 M H_2SO_4 purged with N_2 at room temperature at a sweep rate of 5 mV s^{-1}. The catalyst layer consist of a total metal loading of 28 μg and 5 μL of a mixture of Nafion solution (5 wt.% from Aldrich) and isopropyl alcohol (1:20).

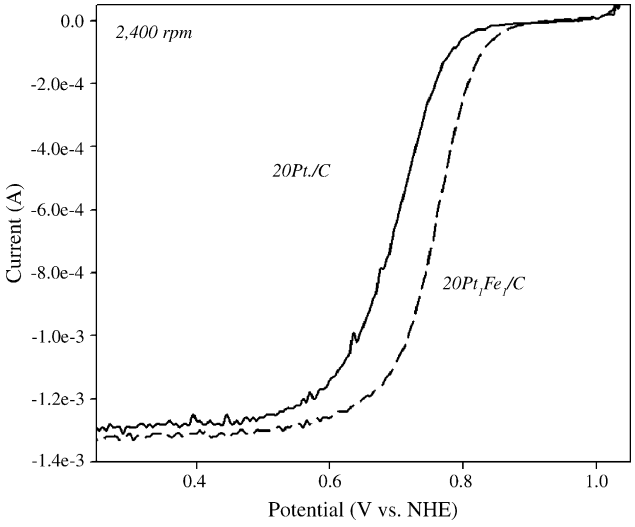

Fig. 2. Polarization curves of Pt and Pt-alloy on rotating disk electrode in 0.3 M H_2SO_4 saturated with O_2 at room temperature and rotated at 2400 rpm. The catalyst layer consist of a total metal loading of 28 μg and 5 μL of a mixture of Nafion solution (5 wt.% from Aldrich) and isopropyl alcohol (1:20).

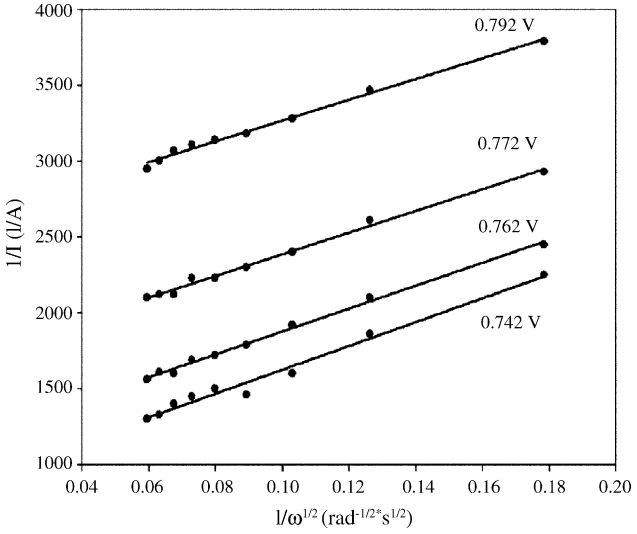

Fig. 3. Koutecky–Levich plots at various potentials measured on $20Pt_1Fe_1/C$ in 0.3 M H_2SO_4 saturated with O_2 at room temperature. The catalyst layer consist of a total metal loading of 28 μg and 5 μL of a mixture of Nafion solution (5 wt.% from Aldrich) and isopropyl alcohol (1:20).

with 50 at.% Pt (i.e., $20Pt_1Co_1/C$) show a modification on the strongly bound H_{UPD} peak. This phenomenon has been attributed to variations in the surface faceting [22,23]. The area under the H_{UPD} desorption peak was used to calculate the electrochemical surface area. A conventional electrochemical method based on the electrical charge required for the hydrogen adsorption–desorption on a polycrystalline Pt surface area (210 μC cm^{-2}) was used [8].

Fig. 2 shows a typical polarization curve of 20% Pt/C and 20% PtFe/C alloy obtained at room temperature in 0.3 M H_2SO_4 saturated with O_2 using a GCRDE at 2400 rpm. At high potentials, the ORR is under the kinetic-diffusion control region. This region is followed by a purely diffusion limited region between 0.55 and 0.1 V versus NHE. A reduction of approximately 80 mV in overpotential occurs for the ORR when Pt is alloyed with iron is clearly seen in the kinetic-diffusion control region. An increase in the rotational speed of the rotating disc electrode results in an increase of the limiting current, due to an increase in the availability of oxygen at the electrode surface. Similar curves are obtained for different alloys.

The Koutecky–Levich (i^{-1} versus $\omega^{-1/2}$) plots obtained for different rotation speeds at potential range between 0.74 and 0.8 V versus NHE are presented in Fig. 3 for Pt_1Fe_1/C. Linear relationships with constant slopes are observed at each potential. The kinetic currents per milligrams of metal at 0.792 V versus NHE for the different catalysts are shown in Fig. 4. The alloys showed an increase in the activity of the ORR. The observed increase of the activity was found to depend on the alloying element and on the platinum to metal (Pt/M) atomic ratio. The catalytic activity increase is in the order of: Pt < Pt-Ni < Pt-V < Pt-Co < Pt-Fe. Thus, Pt alloyed with Fe shows the highest activity while the pure Pt catalyst shows the lowest activity. The alloy composition also controls the activity enhancement. For example, in case of Pt–Co alloy, a higher activity is observed when Pt:Co ratio is 3:1 (20% Pt_3Co_1/C), while for the Pt–Ni alloy higher activity is observed when Pt:Ni ratio is 1:1 (20% Pt_1Ni_1/C).

3.2. Electrochemical and physical characterization of the electrode surface area as a function of time

Fig. 5a and b shows the CVs for 20% Pt/C and 20% Pt_1Co_1/C after consecutive cycling. With cycling, a reduction on the H_{UPD} peak is observed for all catalysts indicating an increase in the metal particle size. The CVs reveal that as

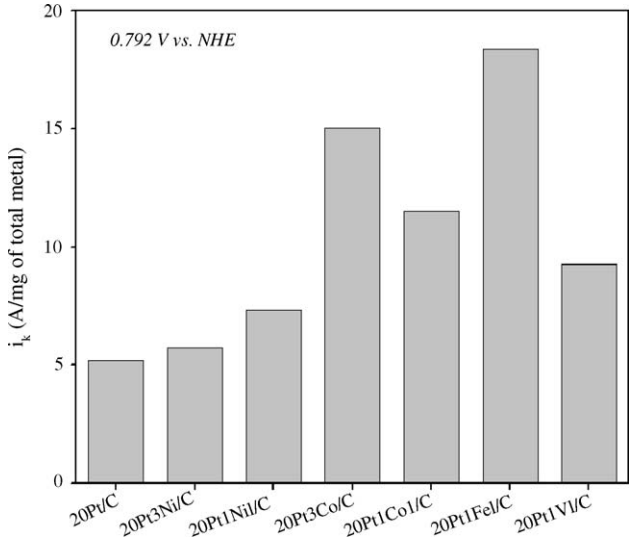

Fig. 4. Kinetically controlled ORR currents at 0.792 V vs. NHE for the different Pt based catalysts.

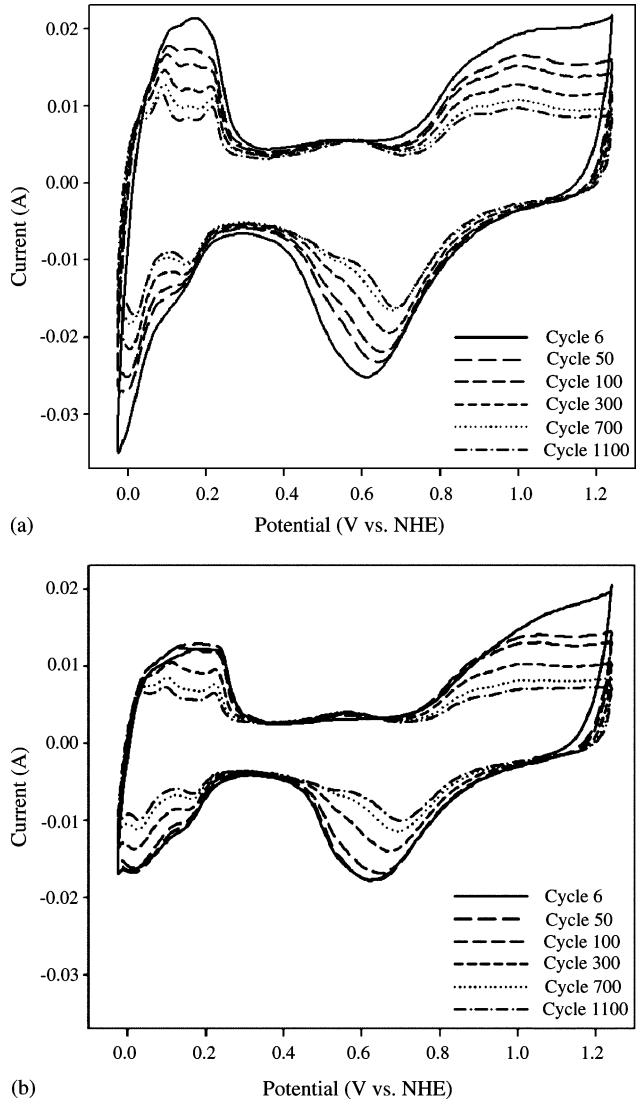

Fig. 5. Voltammograms after consecutive cycling for Pt (a) and Pt_1Co_1 alloy (b) in 0.3 M H_2SO_4 purged with N_2 at room temperature at a sweep rate of 5 mV s^{-1}. The cathode catalyst layer consist of total metal loading of 0.4 mg cm^{-2} and 15 wt.% dry Nafion content on a 10 cm^2 GDL.

the surface area decreases the strong and weak H_{UPD} peaks become more distinct and the fraction of the strong adsorption peak to the total H_{UPD} grows gradually. In the case of pure Pt catalyst, the growth in the separation of the two adsorption peaks and the Pt particle size increase can be correlated, as observed by Kinoshita [24], to an increase in the number of atoms in the (1 1 1) and (1 0 0) crystal phases normalized to the total number of atoms on the surface of the particle. The difference in the extent of the separation of the H_{UPD} observed for pure Pt and Pt-alloys could be due to the dissolution of the alloying metal from the surface of the catalyst particles.

Fig. 6 shows the electrochemical surface area as a function of the cycle number obtained for different Pt catalysts. The surface area was estimated by integrating the H_{UPD} peak and assuming the hydrogen adsorption–desorption process

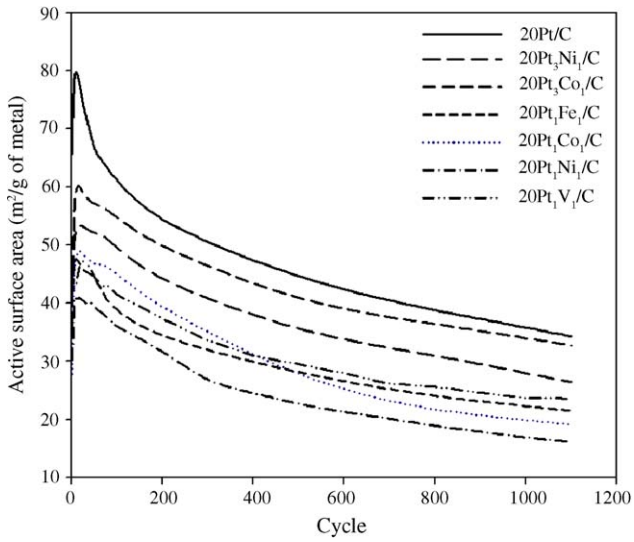

Fig. 6. Electrochemical surface area as a function of cycle for the different Pt catalysts obtained by integrating H_{UPD} peak and assuming hydrogen adsorption–desorption on a polycrystalline Pt surface (210 μC cm^{-2}). The cathode catalyst layer consist of total metal loading of 0.4 mg cm^{-2} and 15 wt.% dry Nafion content on a 10 cm^2 GDL.

occurs on a polycrystalline Pt surface. During the first cycle, the surface area initially increases until it reaches a maximum value. This initial increase occurs due to the initial wetting of the thin Nafion layer covering the catalyst particles. After saturation of the active material with the electrolyte, the surface area starts to decrease. Similar behavior is observed for all tested catalysts where Pt showed initial higher active surface area due to its smaller particle size (2.86 nm) when compared to the initial particle size of the platinum alloy catalyst. As shown in Fig. 6, the surface area of pure platinum and platinum alloy catalyst decreases with the increase of the number of cycles. Note that after 1000 cycles, the surface area of Pt_3Ni_1/C approaches that of Pt/C.

During the CV measurements, the catalysts were exposed to extremely corrosive conditions. By polarizing the catalyst in acidic media, the corrosion of the carbon support results in a loss of the active surface area due to particle sintering [25,26]. Different mechanisms of Pt dissolution–redeposition on the catalyst surface and Pt migration through the surface have also been suggested [9–13,27] to explain the increase of the catalyst particle with time.

In the case of platinum alloys, both the non-noble metal particles and Pt dissolve into the electrolyte. Then the dissolved Pt redeposits on the surface of larger particles, a phenomenon known as Ostwald ripening [15]. After 1000 cycles, as shown in Fig. 6, the highest loss of surface area (∼57%) from the pure platinum catalyst indicates that the processes of Ostwald ripening, Pt particle migration and sintering occur at a higher rate when compared to the redeposition and particle sintering of platinum alloys. Whereas, the lowest surface area loss (∼43%) was observed for the catalyst with a non-noble metal content of 25 at.% (i.e., 20% Pt_3Co_1/C and 20% Pt_3Ni_1/C).

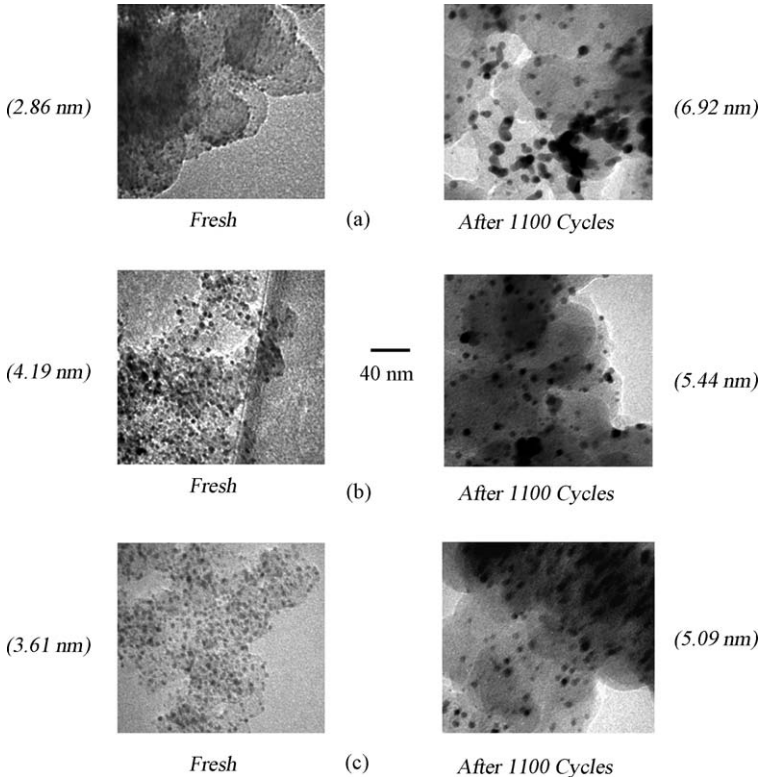

Fig. 7. TEM images of 20Pt/C (a), 20Pt_3Ni_1/C (b) and 20Pt_3Co_1/C (c) before and after consecutive cycling in 0.3 M H_2SO_4 purged with N^2 at room temperature.

Fig. 7a–c shows the TEM images of 20% Pt/C, 20% Pt_3Ni_1/C and 20% Pt_3Co_1/C, respectively. From these images, it is observed that there is a considerable particle growth consistent with the surface area decrease observed in Fig. 6.

3.3. Accelerated durability test

In our previous work, it was shown that higher degradation of the Pt-alloys is observed at high potentials, more precisely in the region where the ORR is kinetically controlled [20]. For this reason, we concentrated our efforts in studying the durability of the catalysts at 0.8 and 0.9 V versus NHE, where the major damage is expected to occur during normal fuel cell operation.

Fig. 8 shows the change in ORR current as a function of time at 0.8 V versus NHE for three selected catalysts: 20% Pt/C, 20% Pt_3Ni_1/C and 20% Pt_3Co_1/C. The insert shows the data of all materials tested at 0.8 V versus NHE. At the beginning of the ADT the current initially increases until it reaches a maximum value. This initial increase occurs as part of the initial wetting and saturation of the thin Nafion layer covering the catalyst particles. The amount that the initial peak intensity increases is determined by correlating the initial activity and the particle size of the catalyst. Once the current reaches the maximum, it starts to decrease rapidly for the first 100 h until it reaches a slow, but steady decay. Shown on the insert of Fig. 8, the highest initial current was observed for 20% Pt_1Fe_1/C, which correlates to the activity observed in Fig. 4. However, after reaching steady state, the activity decay is highest when compared to the other alloy catalysts. Fig. 8 shows that after the initial decay and once the current have reached steady state (after 100 h), 20% Pt/C shows the lowest activity in agreement with the results presented in Fig. 4.

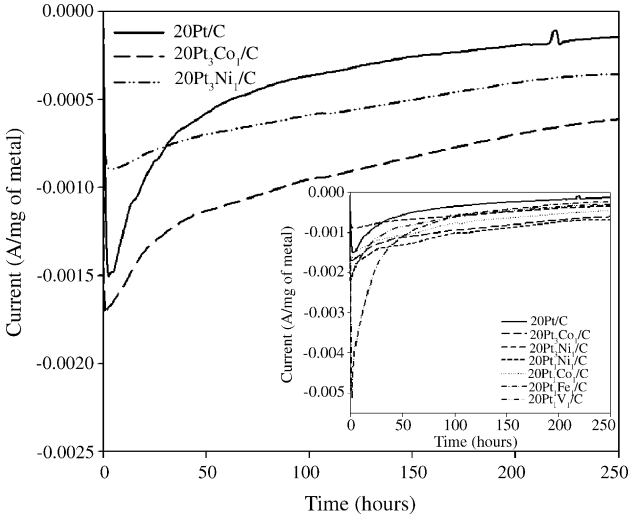

Fig. 8. Polarization data as a function of time for the different Pt based catalysts for a fixed potential of 0.8 V vs. NHE in 0.3 M H_2SO_4 saturated with O_2 at room temperature. The cathode catalyst layer consist of total metal loading of 0.4 mg cm^{-2} and 15 wt.% dry Nafion content on a 10 cm^2 GDL.

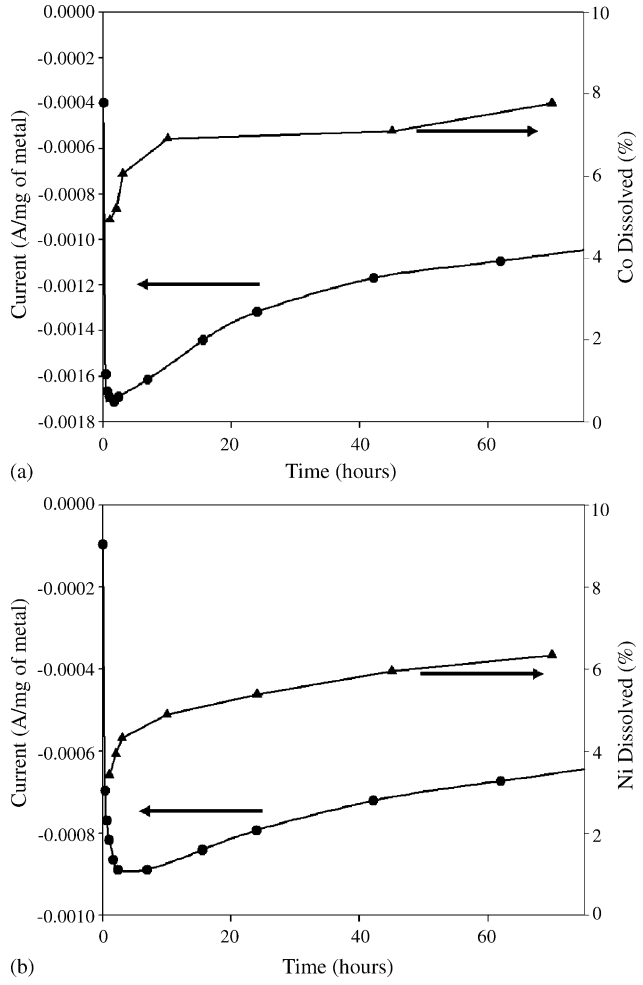

Fig. 9. Polarization data and non-noble metal dissolution data as a function of time for $20Pt_3Co_1/C$ (a) and $20Pt_3Ni_1/C$ (b) fixed at a potential of 0.8 V vs. NHE. The cathode catalyst layer consist of total metal loading of 0.4 mg cm^{-2} and 15 wt.% dry Nafion content on a 10 cm^2 GDL.

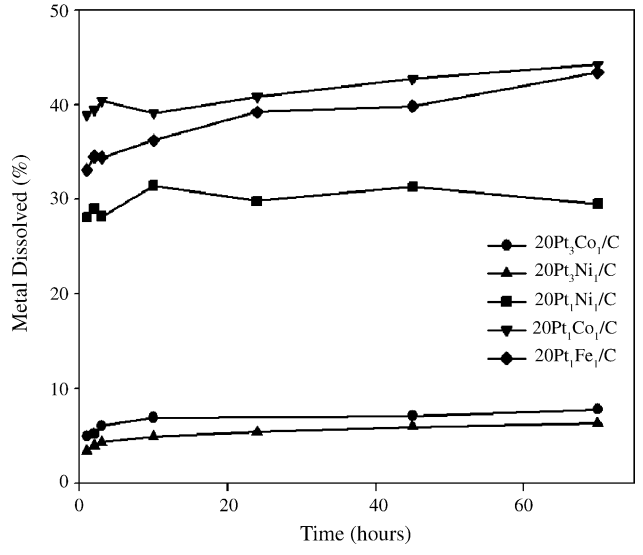

Fig. 10. Non-noble metal dissolution data as a function of time for the different Pt-alloy catalysts at a potential fixed to 0.8 V vs. NHE.

Fig. 9a and b shows the ORR current as a function of time. These figures also show the percentage losses of Co and Ni metals dissolved from 20% Pt_3Co_1/C and 20% Pt_3Ni_1/C alloy samples polarized at 0.8 V versus NHE. Since both studies were done in the same time domain, the results indicate a strong correlation between the amount of metal dissolved in the electrolyte and the value of the ORR current decay. The main cause for the initial rapid decay of the catalytic activity for the Pt-alloys is the metal dissolution. However, as can be observed in Fig. 8, the initial decay is faster for pure Pt catalyst, which indicates a different mechanism in the activity decay for the pure Pt catalysts.

Fig. 10 shows the dissolution rate estimated for different Pt-alloy catalysts at 0.8 V versus NHE. The highest metal loss was estimated for the samples with a Pt to non-noble metal ratio of 1:1. As expected, the metal loss in the samples with a Pt to non-noble metal ratio of 3:1 is lower than that estimated for 1:1 Pt/M ratio. In case of 1:1 Pt/M ratio, Pt–Ni alloy shows the lowest metal dissolution followed by

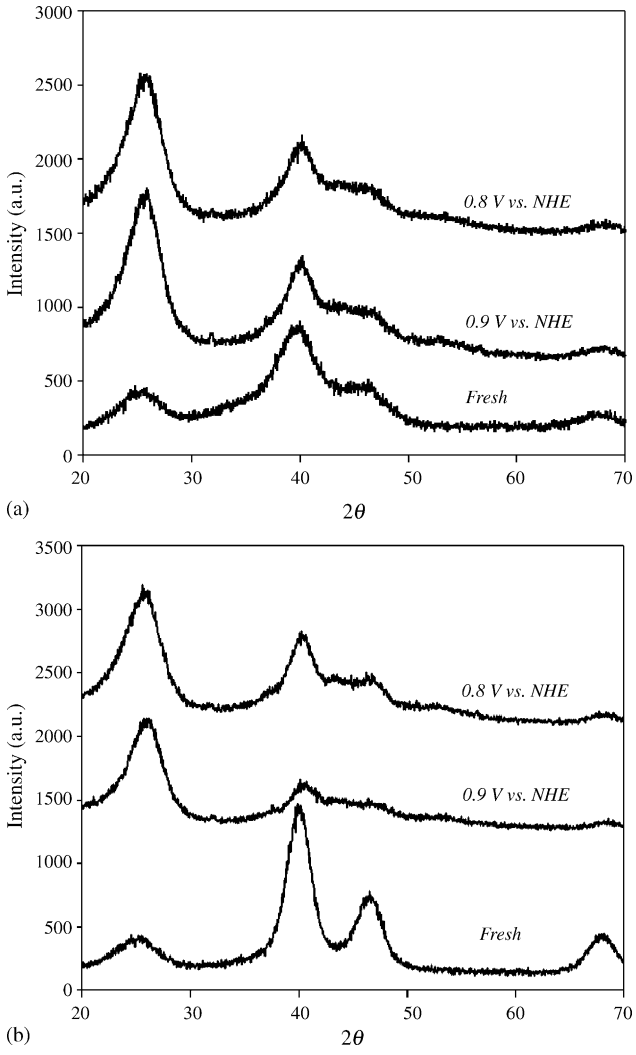

Fig. 11. XRD patterns of Pt/C (a) and Pt_3Ni_1/C (b) fresh and after 480 h of ADT at 0.8 and 0.9 V vs. NHE.

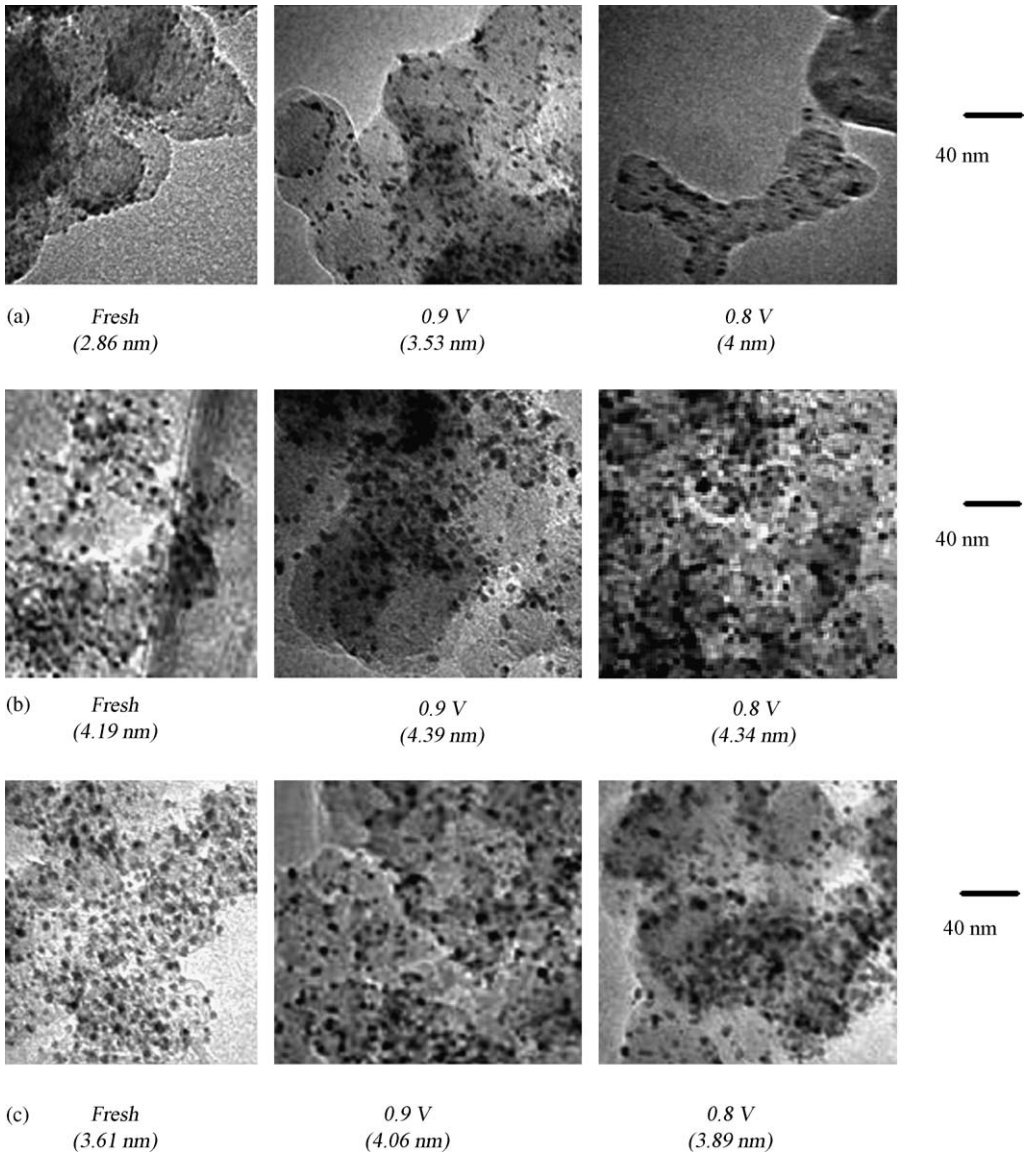

Fig. 12. TEM images of 20Pt/C (a), 20Pt_3Ni_1/C (b) and 20Pt_3Co_1/C (c) before and after ADT test at 0.9 and 0.8 V vs. NHE.

iron. However, higher dissolution of Fe can be expected after 100 h, since according to Fig. 10, the dissolution rate observed for Co and Ni is slower than that of Fe. According to the mixed potential theory, the corrosion potential should be between the standard hydrogen reduction potential (0 V versus SHE) and the metal reversible potential (−0.250, −0.277 and −0.440 V versus NHE for Ni, Co and Fe, respectively). Since the applied potential in the ADT is more positive than the corrosion potential, the oxidation overpotential of the metals increases as the corrosion potential decreases thereby increasing the driving force for the metal dissolution reaction.

The powder X-ray diffraction patterns of the Pt/C and the Pt_3Ni_1/C are given in Fig. 11a and b, respectively. The X-ray pattern of the fresh sample was taken using the received catalyst powder. In the case of the tested sample, the X-ray pattern was taken using the powders spread over the GDL. The diffraction peak at 2θ of 25° shown in the catalysts is associated with the (0 0 2) plane of the hexagonal structure characteristic of carbon blacks [28]. The increase in magnitude observed in the carbon peak intensity for the tested samples can be explained by the contribution of the carbon on the microporous layer on the GDL. The characteristic diffraction peaks of the face centered cubic structure are detected in the platinum supported carbon catalyst samples. The diffraction peaks at 2θ values of 40, 47 and 67 are associated with the Pt (1 1 1), (2 0 0) and (2 2 0) planes, respectively. Among the diffraction peaks of Pt-alloys, the typical peaks corresponding to the unalloyed metals are not detected. However, in the case of the Pt-alloy catalysts, the diffraction peak (1 1 1) of Pt shifts slightly to higher Bragg angles. The shift indicates a decrease in the lattice constant in the presence of the alloying metal. Such evidence accounts for the formation of Pt-alloy in the catalyst. The XRD patterns of the Pt-alloy catalyst after the ADT analysis at 0.8 and 0.9 V versus NHE showed lattice

constants similar to those of pure Pt catalyst (see Fig. 11b). This result suggests that the non-noble alloying metal has dissolved in the electrolyte and supports the fact that mechanism of non-noble metal dissolution causes the decline in the performance of the Pt-alloy catalysts. Similar results have been observed by Roh et al. for Pt–Cu–Fe alloy [16], and by Yu et al. for Pt–Co alloys on a carbon substrate [29].

Fig. 12a–c shows the TEM images and the average particle size of 20% Pt/C, 20% Pt_3Co_1/C and 20% Pt_3Ni_1/C, respectively. Fig. 12a shows the particle size of platinum estimated at 0.8 and 0.9 V versus NHE increases from 2.86 to 4.00 and 3.53 nm, respectively, after 480 h of ADT analysis. The observed increase in Pt particle size is probably due to the crystallite migration mechanism, which is explained by the migration and aggregation platinum particles to form larger particles. Wilson et al. have reported that Pt catalyst average particle size calculated from the particle size population distribution plot increases from 1.7 to 2.5 nm after 1300 h of continuous operation in a PEM fuel cell, accounting for a Pt loss in surface area of 32% [17]. On the other hand, TEM of Pt-alloy catalysts (Fig. 12b and c) shows an increase of particle size from 4.19 to 4.34 and 4.39 nm for 20% Pt_3Ni_1/C and from 3.61 to 3.89 and 4.06 nm for 20% Pt_3Co_1/C after 480 h of ADT analysis. The increase in the particle size of the Pt-alloy catalysts is almost negligible when compared to

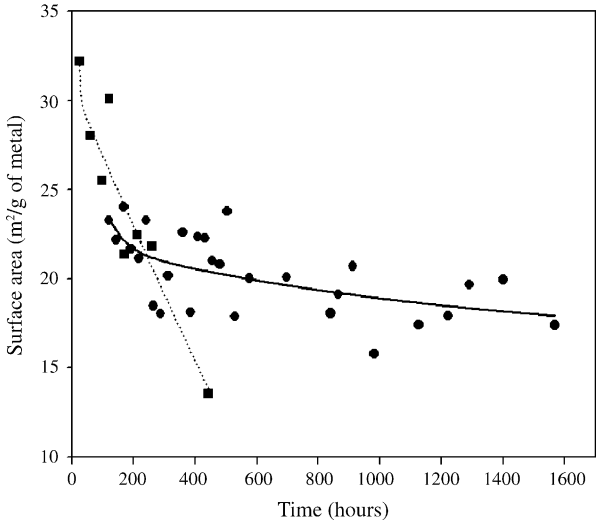

Fig. 13. Electrochemical surface area as a function of time for the 20Pt/C (squares) and 20Pt_3Co_1/C (circles) catalysts obtained by integrating H_{UPD} peak and assuming hydrogen adsorption–desorption on a polycrystalline Pt surface (210 μC cm^{-2}). The cathode catalyst layer consist of total metal loading of 0.4 mg cm^{-2} and 25 wt.% dry Nafion content. The anode catalyst layer consist of commercial E-TEK electrode (30 wt.% Pt) with a loading of 0.5 mg cm^{-2} of Pt. Cell size: 10 cm^2.

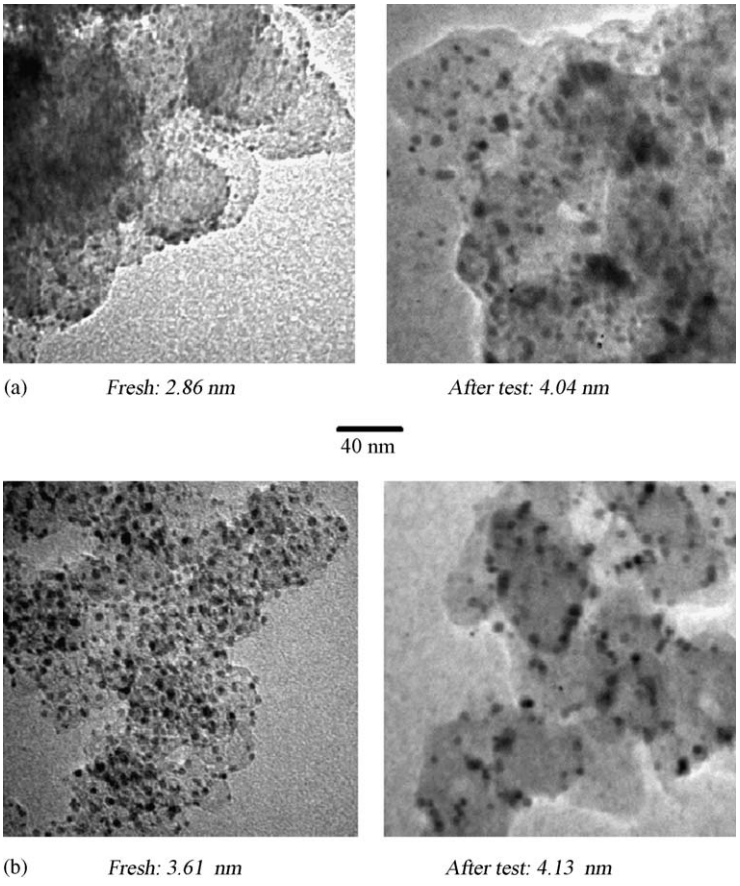

Fig. 14. TEM images of 20Pt/C (a) and 20Pt_3Co_1/C (b) before and after the fuel cell testing.

the decay in ORR current. These results can be explained by the increased sintering resistance offered by the alloying elements (i.e., the anchor effects of the alloying element on the carbon substrates) when compared with pure Pt catalysts. Similar results are reported in the literature for Pt–Ni and Pt–Fe alloys [20,30].

3.4. Fuel cell testing

20% Pt_3Co/C catalyst showed the highest performances and stability in the ADT testing. While the 20% Pt/C exhibits different deterioration mechanisms and was considered as the baseline in our fuel cell experiments. Thus, to correlate the performance of the catalysts in fuel cells with our ADT results, 20% Pt/C and 20Pt_3Co/C were selected as catalysts to be tested in the fuel cell setup. They were tested by applying a constant load of 1 A cm^{-2} and by monitoring the potential as a function of time. Periodically, the active surface area was estimated by using a CV. The initial potentials under the applied load were 0.615 and 0.620 V versus NHE for 20% Pt/C and 20% Pt_3Co/C. The testing was terminated when the potential dropped to 0.49 V versus DHE. In the case of 20% Pt/C, the experiment was stopped after 400 h of operation. Similar degradation times were observed and reported in the literature for experiments performed under similar conditions and pure Pt/C used as the catalyst [31]. In the case of 20% Pt_3Co/C, the cell was stopped at 1600 h.

Fig. 13 shows the electrochemical surface area as a function of time for the 20% Pt/C and 20% Pt_3Co/C catalysts. As shown in Fig. 13, the loss in surface area is considerable for the Pt catalysts. On the other hand, the loss in active surface area is not as drastic in the case of Pt–Co alloy, despite the fact that the cell testing was performed for a period nearly four times as long.

Fig. 14a and b shows the TEM images of 20% Pt/C and 20% Pt_3Co/C catalyst particles before and after the fuel cell testing. As shown in Fig. 14, there is a considerable particle growth in the case of the Pt catalyst that is consistent with

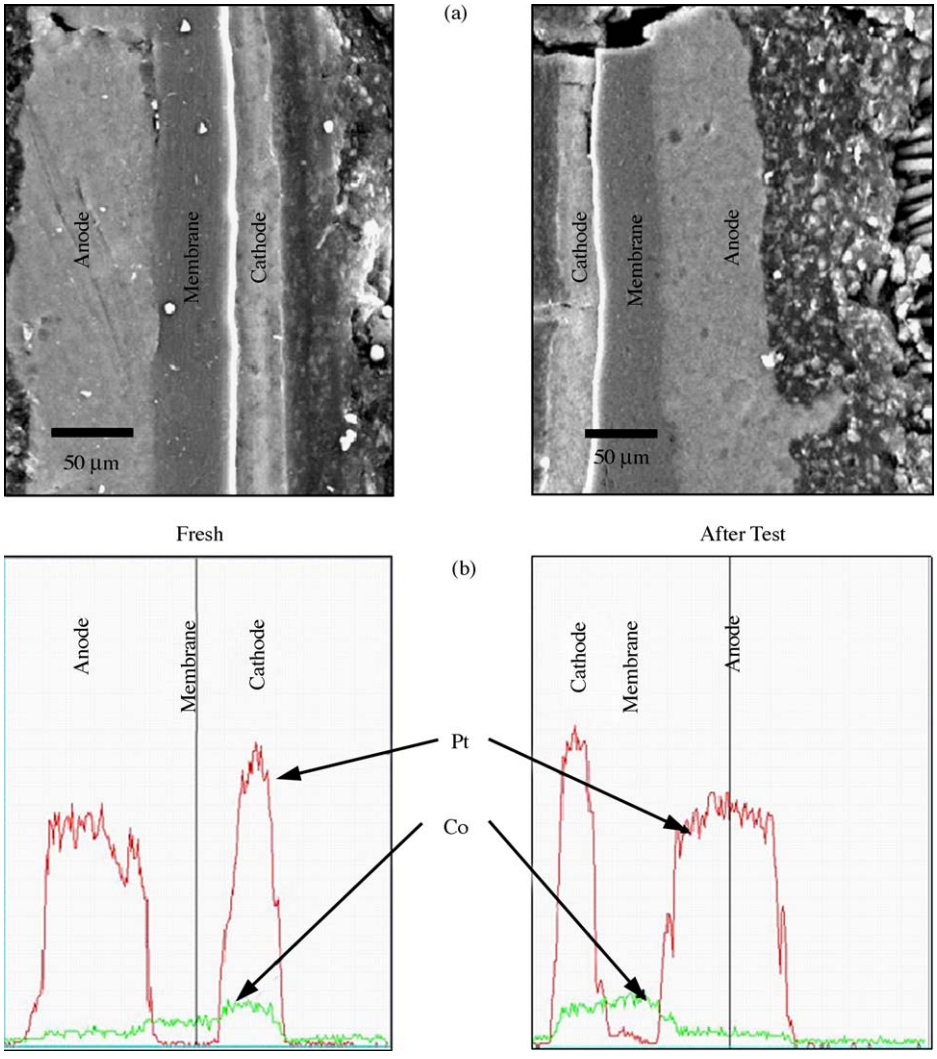

Fig. 15. BSEM image (a) and EMPA cross-section line scan (b) of the fresh and after test MEA containing 20Pt_3Co_1/C on the cathode side.

a surface area decrease. The same behavior was observed during the accelerated deterioration test.

Fig. 15a and b shows the BSEM image and EMPA cross-section line scan of the fresh and post-cell test of the MEA, which contains 20% Pt_3Co/C catalyst on the cathode side. Five distinct layers can be identified: the anode GDL, the ETEK commercial Pt anode, the Nafion membrane, the cathode catalyst layer and the cathode GDL.

From the change in the contrast provided by the BSEM, it is difficult to distinguish any small changes in the concentration of the cobalt through the cross-section. Using the EMPA cross-section line scan one can qualitatively measure the intensity of the metal distribution across the MEA and compare the results of the fresh and tested MEA. Fig. 15 shows that the EMPA cross-section line scan taken for the tested sample indicates that there is not a significant signal coming from Pt in the membrane, meaning that Pt is stable in the system. However, when moving from the cathode side towards the membrane, an increase in the Co signal is observed indicating dissolution of the non-noble metal (Co) and its diffusion through the Nafion membrane.

4. Conclusion

The influence of the alloying metal on the catalytic, corrosion and sintering properties of Pt based catalysts was studied. The initial activity was found to be the highest for the Pt-Fe catalyst and lowest for pure Pt catalyst. Accelerated durability test was used to study the stability of the catalysts. The observed decay in performance of the catalyst was explained by two key mechanisms: particle migration (for the pure Pt catalyst) and Ostwald ripening (for the Pt-alloy catalyst). The results of the ORR current measurement indicated a higher loss in the performance during the first 100 h of testing due to the dissolution of the non-noble metal for Pt-alloys and particle sintering for Pt catalyst. Fuel cell testing with the catalysts indicated that the stability of Pt catalyst improves with the addition of an alloying element. However, dissolution of the alloying element followed by diffusion into the membrane was observed in the cross-sectional studies by electron microprobe analysis of the post-cell test MEA. It is envisaged that this phenomenon will lead to additional deterioration in the long-term performance of the membrane and fuel cell.

Acknowledgement

The financial support of the National Science Foundation Industry/University Cooperative Research for Fuel Cells at the University of South Carolina is gratefully acknowledged.

References

[1] T.R. Ralph, M.P. Hogarth, Platinum Metal Rev. 46 (2002) 3–14.
[2] E. Antolini, Mater. Chem. Phys. 78 (2003) 563–573.
[3] V. Jalan, E.J. Taylor, J. Electrochem. Soc. 130 (1983) 2299–2302.
[4] M. Min, J. Cho, K. Cho, H. Kim, Electrochim. Acta 45 (2000) 4211–4217.
[5] S. Mukerjee, S. Srinivasan, J. Electroanal. Chem. 357 (1993) 201–224.
[6] B.C. Beard, P.N. Ross, J. Electrochem. Soc. 137 (1990) 3368–3374.
[7] S. Mukerjee, S. Srinivasan, M.P. Soriaga, J. Electrochem. Soc. 142 (1995) 1409–1422.
[8] T. Toda, H. Igarashi, H. Uchida, M. Watanabe, J. Electrochem. Soc. 146 (1999) 3750–3756.
[9] A. Honji, T. Mori, K. Tamura, Y. Hishinuma, J. Electrochem. Soc. 135 (1988) 355–359.
[10] P. Bindra, S. Clouser, E. Yeager, J. Electrochem. Soc. 126 (1979) 1631–1632.
[11] G.A. Gruver, R.F. Pascoe, H.R. Kunz, J. Electrochem. Soc. 127 (1980) 1219–1224.
[12] A.C.C. Tseung, S.C. Dhara, Electrochim. Acta 20 (1975) 681–683.
[13] K.F. Blurton, H.R. Kunz, D.R. Rutt, Electrochim. Acta 23 (1978) 183–190.
[14] K.T. Kim, Y.G. Kim, J.S. Chung, J. Electrochem. Soc. 142 (1995) 1531–1538.
[15] M. Watanabe, K. Tsurumi, T. Mizukami, T. Nakamura, P. Stonehart, J. Electrochem. Soc. 141 (1994) 2659–2668.
[16] W. Roh, J. Cho, H. Kim, J. Appl. Electrochem. 26 (1996) 623–630.
[17] M.S. Wilson, F.H. Garzon, K.E. Sickafus, S. Gottesfeld, J. Electrochem. Soc. 140 (1993) 2872–2877.
[18] T. Toda, H. Igarashi, M. Watanabe, J. Electroanal. Chem. 460 (1999) 258–262.
[19] L.J. Wan, T. Moriyama, M. Ito, H. Uchida, M. Watanabe, Chem. Commun. (2002) 58–59.
[20] H.R. Colón-Mercado, H. Kim, B.N. Popov, Electrochem. Commun. 6 (2004) 795–799.
[21] U.A. Paulus, T.J. Schmidt, H.A. Gasteiger, R.J. Behm, J. Electroanal. Chem. 495 (2001) 134–145.
[22] M.T. Paffett, J.G. Beery, S. Gottesfeld, J. Electrochem. Soc. 135 (1988) 1431–1436.
[23] U.A. Paulus, A. Wokaun, G.G. Scherer, T.J. Schmidt, V. Stamenkovic, N.M. Markovic, P.N. Ross, Electrochim. Acta 47 (2002) 3787–3798.
[24] K. Kinoshita, J. Electrochem. Soc. 137 (1990) 845–848.
[25] M. Uchida, Y. Aoyama, M. Tanabe, N. Yanagihara, N. Eda, A. Ohta, J. Electrochem. Soc. 142 (1995) 2572–2576.
[26] G.A. Gruver, J. Electrochem. Soc. 125 (1978) 1719–1720.
[27] R.M. Darling, J.P. Meyers, J. Electrochem. Soc. 150 (2003) A1523–A1527.
[28] T. Ungár, J. Gubieza, G. Tichy, C. Pantea, T.W. Zerda, Compos. Part A 36 (2005) 431–436.
[29] P. Yu, M. Pemberton, P. Plasse, J. Power Sources 144 (2005) 11–20.
[30] Z. Wei, H. Guo, Z. Tang, J. Power Sources 62 (1996) 233–236.
[31] A.A. Kulikovsky, H. Scharmann, K. Wippermann, Electrochem. Commun. 6 (2004) 75–82.